14. Shannon, R. D. Revised effective ionic radii and systematic studies of interatomic distances in halides and chalcogenides. *Acta Crystallogr. A* **32,** 751–767 (1976).
15. Hansen, M. (ed.) *Constitution of Binary Alloys* (McGraw-Hill, New York, 1958).
16. Emsley, J. (ed.) *The Elements* (Clarendon, Oxford, 1994).
17. Tanaka, H., Takahashi, I., Kimura, M. & Sobukawa, H. in *Science and Technology in Catalysts 1994* (eds Izumi, Y., Arai, H. & Iwamoto, M.) 457–460 (Kodansya-Elsevier, Tokyo, 1994).
18. Tanaka, H., Tan, I., Uenishi, M., Kimura, M. & Dohmae, K. in *Topics in Catalysts* (eds Kruse, N., Frennet, A. & Bastin, J.-M.) Vols 16/17, 63–70 (Kluwer Academic, New York, 2001).

Supplementary Information accompanies the paper on *Nature*'s website (http://www.nature.com/nature).

Acknowledgements

We thank M. Misono and N. Mizuno for their advice on catalyst research.

Competing interests statement

The authors declare that they have no competing financial interests.

Correspondence and requests for materials should be addressed to Y.N. (e-mail: yasuon@spring8.or.jp).

A satellite geodetic survey of large-scale deformation of volcanic centres in the central Andes

Matthew E. Pritchard & Mark Simons

Seismological Laboratory, Division of Geological and Planetary Sciences, California Institute of Technology, Pasadena, California 91125, USA

Surface deformation in volcanic areas usually indicates movement of magma or hydrothermal fluids at depth. Stratovolcanoes tend to exhibit a complex relationship between deformation and eruptive behaviour[1]. The characteristically long time spans between such eruptions requires a long time series of observations to determine whether deformation without an eruption is common at a given edifice. Such studies, however, are logistically difficult to carry out in most volcanic arcs, as these tend to be remote regions with large numbers of volcanoes (hundreds to even thousands). Here we present a satellite-based interferometric synthetic aperture radar (InSAR) survey of the remote central Andes volcanic arc, a region formed by subduction of the Nazca oceanic plate beneath continental South America. Spanning the years 1992 to 2000, our survey reveals the background level of activity of about 900 volcanoes, 50 of which have been classified as potentially active[2,3]. We find four centres of broad (tens of kilometres wide), roughly axisymmetric surface deformation. None of these centres are at volcanoes currently classified as potentially active, although two lie within about 10 km of volcanoes with known activity. Source depths inferred from the patterns of deformation lie between 5 and 17 km. In contrast to the four new sources found, we do not observe any deformation associated with recent eruptions of Lascar, Chile[4,5].

We have created radar interferograms imaging about 900 of the approximately 1,100 catalogued volcanic edifices in the central Andes[2] (Fig. 1). Included in our study are several silicic calderas and geothermal fields. Temporal coverage is variable—for some locations, ERS 1 and 2 (European Space Agency remote-sensing satellites) radar data are available from 1992 to 2000, but only four years of data are available for a few volcanoes.

We infer four major sources of deformation from the InSAR data. We find that Uturuncu, a stratovolcano in Bolivia, has a maximum deformation rate in the radar line-of-sight (LOS) direction, U_{LOS}, of 1–1.5 cm yr^{-1} (Fig. 2). An area in southern Peru about 2.5 km east of the volcano Hualca Hualca and 7 km north of the active volcano Sabancaya is inflating with U_{LOS} of about 2 cm yr^{-1}. A third inflationary source (with $U_{LOS} = 1$ cm yr^{-1}) is not associated with a volcanic edifice. This third source is located 11.5 km south of Lastarria and 6.8 km north of Cordon del Azufre on the border between Chile and Argentina, and is hereafter called 'Lazufre'. Robledo caldera, in northwest Argentina, is subsiding with U_{LOS} of 2–2.5 cm yr^{-1}. Because the inferred sources are more than a few kilometres deep, any complexities in the source region are damped such that the observed surface deformation pattern is smooth. We find no measurable deformation at volcanoes with small eruptions or fumarolic activity during the period when radar observations were made—Ubinas (in Peru) or Guallatiri, Irruputuncu and Ojos del Salado (in Chile)[6].

It is possible that other volcanoes are deforming at rates below our detection threshold. We quantify our sensitivity to deformation by comparing temporally overlapping interferograms, and by consideration of previous analyses of InSAR accuracy[7]. We estimate that we can detect a signal of 1–2 cm amplitude that is at least 10 km in spatial extent. Differentiating such a signal from atmospheric noise within a single interferogram is difficult, but is possible by comparing multiple interferograms, as well as multiple edifices within an interferogram. Owing to decorrelation of the radar signal near many of the volcano summits, our survey is not very sensitive to localized near-surface deformation, as seen for example in the Galapagos[8]. Because the longest interferograms that we can form for most regions span about 5 yr (limited by data availability and maintaining interferometric coherence), we can detect average deformation rates exceeding 4 mm yr^{-1}.

We model the observed surface deformation as resulting from a spherical point-source of volume change, embedded in either a homogeneous or layered elastic crust. For each volcano, we simultaneously invert data from as many different time periods and satellite tracks as possible, assuming a single source location. We solve for the volume change in each interferogram separately. For our inversions, we use the Neighbourhood Algorithm global search approach, which can find multiple local minima and a range of acceptable models[9]. The misfit function is usually peaked near the best estimate, but because of the data noise and non-uniqueness of the problem, we instead choose to use the width of the misfit function to estimate a range of acceptable values.

We consider how three different seismically derived one-dimensional layered elastic models[10,11] affect estimates of source parameters. We incorporate the effects of topography upon source depth by using a different source depth for each pixel depending upon local elevation[12]. Our experiments with different elastic structures, topography, and the trade-off between source depth and volume change indicate a range of possible source depths for each centre of deformation spanning a few kilometres.

From north to south, the inferred source depths (below sea level) are: 11–13 km at Hualca Hualca; 15–17 km for Uturuncu; 6–8 km for Lazufre; and 4.5–6 km at Robledo. Thus, we find no obvious pattern in source depth within this volcanic arc. The fit of the models to the data is generally good (root mean square, r.m.s. < 1 cm, Fig. 2), although a consistent residual northeast of Hualca Hualca might indicate localized subsidence, and the oblong shape of the Lazufre deformation pattern suggests the need for a non-spherical source.

The rate of volume change seems to be time-dependent at Uturuncu, Lazufre and Robledo, whereas the deformation rate at Hualca Hualca seems constant within measurement error (Fig. 3). At Lazufre, no deformation is apparent before early 1998 in two averaged interferograms, but there is a clear signal in three later interferograms. The temporal coverage is insufficient to resolve whether the start of deformation was abrupt or gradual. At Uturuncu, there is also a slight increase in inflation rate after early

1998. It could be coincidental that the two centres have an increased rate of inflation at roughly the same time, but we note that a $M_w = 7$ subduction zone earthquake occurred near the time of the increase (30 January 1998, Fig. 1). Correlations between unrest at volcanic centres and regional earthquakes have been documented before[13]. At Robledo, the rate of subsidence seems to be decreasing with time.

Even at well-studied volcanoes, the cause of the deformation is often ambiguous. Given the paucity of relevant studies in the central Andes, we emphasize that the cause of deformation we observe is not known. Inflation at Hualca Hualca, Uturuncu and Lazufre could be caused by injection of magma from depth, melting of crustal rock from a previous injection, or build-up of pressure from a hydrothermal system. Given the inferred 15–17 km source depth for deformation at Uturuncu, the source is probably magmatic, not hydrothermal in nature. This source is part of the Altiplano–Puna Magmatic Complex[14], and may be related to a region of low seismic velocity inferred to indicate a zone of partial melt at 19 km (ref. 15).

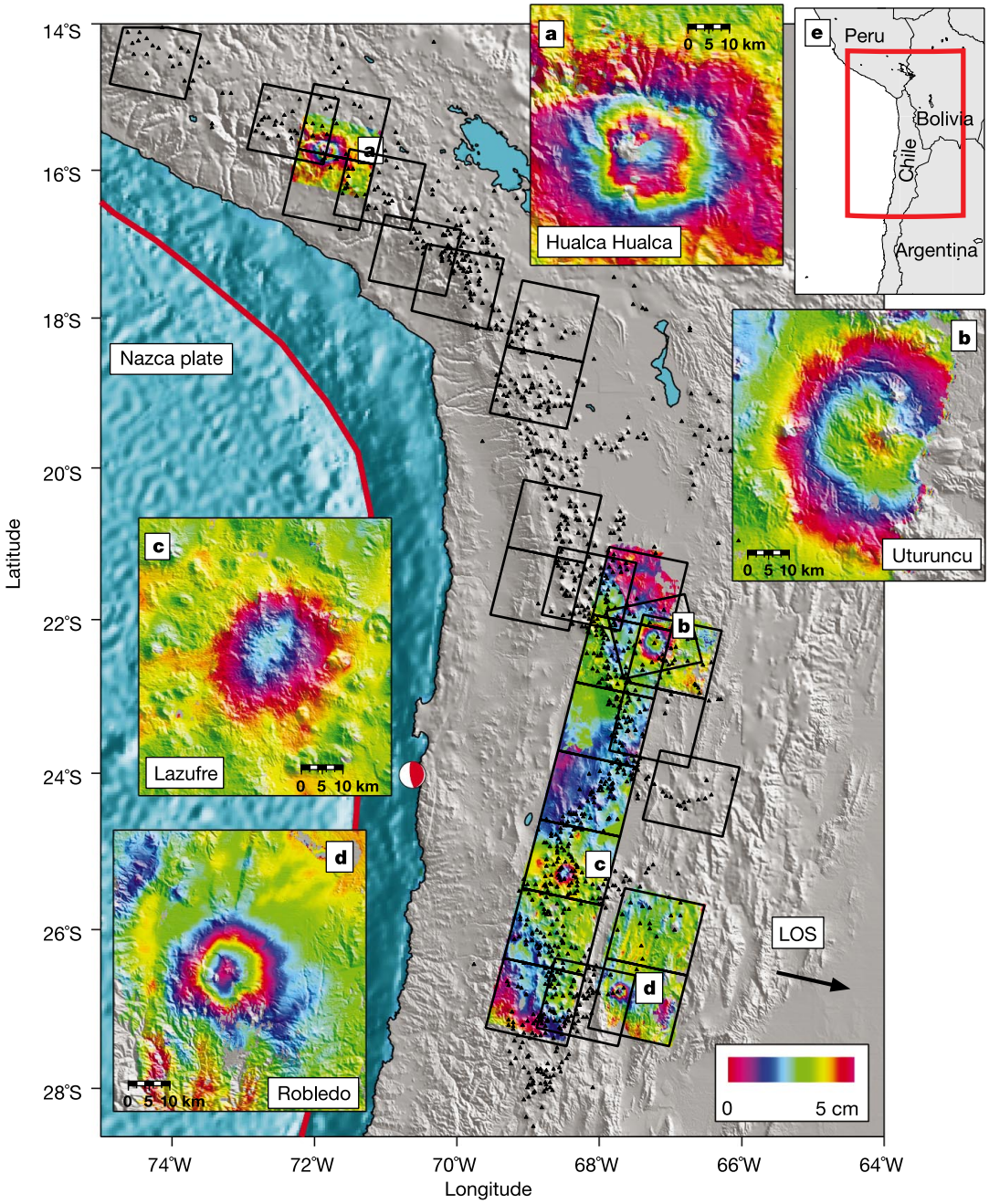

Figure 1 Shaded relief topographic map of the central Andes. The radar frames used in this study are shown (black squares). Black triangles show the 1,113 potential volcanic edifices[2]. The red line in the ocean is the location of the trench. Colour shows interferograms (draped over shaded relief) from this study indicating active deformation—each colour cycle corresponds to 5 cm of deformation in the radar line-of-sight (LOS) direction. Arrow shows radar LOS direction from ground to spacecraft, which is inclined 23° from the vertical. The red and white circle indicates the location of the $M_w = 7$ subduction zone earthquake mentioned in the text that is temporally correlated with increases in the rates of inflation at Uturuncu and Lazufre. Inset maps provide detailed views of the centres of volcanic deformation: **a**, Hualca Hualca, Peru, time span June 1992–April 1996 (3.9 yr); **b**, Uturuncu, Bolivia, time span May 1996–December 2000 (4.6 yr); **c**, Lazufre, time span May 1996–December 2000 (4.6 yr), all of which are inflating; and **d**, Robledo, time span May 1996–October 2000 (4.4 yr), in northwest Argentina, which is deflating. **e**, Red box places main figure in context.

Lazufre and Robledo also lie near regions with low seismic velocities[10]. The deformation source near Hualca Hualca could be related to activity at Sabancaya, even though it is 7 km away. During the 1990 eruptions of Sabancaya, a concentration of earthquakes was located between 4–7 km depth in about the same region as our inferred deformation source[16]. A large distance between an eruptive centre and the magma chamber has been inferred elsewhere; for example, in Alaska, where the 1912 Novarupta eruption was at least partially fed by a magma chamber beneath Mt Katmai 10 km distant[17]. Lazufre also lies more than 7 km from the nearest potentially active volcano. This inferred deformation source could plausibly feed either of the nearby volcanoes, or—as it lies within a topographic depression—it could represent an incipient caldera. Subsidence at the southernmost source, Robledo, is most probably caused by cooling or crystallization of a magma body or hydrothermal activity, and not by lateral draining of magma, because no deformation signal from such magma movement is seen.

Lascar, Chile, is currently the most active volcano in the central Andes and has had several eruptions during the period when InSAR data are available. We do not observe any deformation at Lascar in interferograms spanning the eruptions in April 1993, December 1993, and July 2000, or those spanning other periods of mild vulcanian and fumarolic activity (Fig. 4). In the co-eruptive interferograms, there is a small region of interferometric decorrelation around the edifice, but even so, the large expected deformation signal from the estimated volume of material erupted cannot hide at shallow depths. However, if the source is deep, the corresponding surface deformation signal could be below our detection threshold, thereby placing a constraint on the minimum chamber depth. Assuming a spherical source in an elastic half space and a range in volume of erupted material (10^8 m^3 for April 1993; 10^6–10^7 m^3 for December 1993 and July 2000)[18], the minimum depths below local relief for the April 1993 eruption is 20–25 km, and 5–12 km for the December 1993 and July 2000 eruptions. Petrological estimates of the magma chamber depth range from 5–6 km (ref. 19) to 12–22 km (ref. 20). Alternatively, the absence of surface deformation could indicate that the magma plumbing system (particularly the vertical conduit) behaved rigidly and did not deform during the eruption. We note that gravity measurements at several other volcanoes appear to indicate magma movements without surface deformation[21–23]. Finally, the lack of surface deformation may result from temporally aliased observations related to the cyclic eruptive style of Lascar. At Lascar, a lava dome grows within the crater, cools and subsides, inhibiting degassing and building pressure within the chamber until eruption[4]. In each case, our co-eruptive interferograms begin before the subsidence and pressure build-up commenced, so that pre-eruptive inflation of Lascar could have been approximately balanced by post-eruptive collapse, giving little net deformation in the interferogram. All three alternatives are viable, with further work required before one explanation can be favoured.

Our survey suggests the need for monitoring and hazard assessment near the four sources of deformation. Potential hazards from eruption include mudflows (triggered by melting snow), landslides, pyroclastic flows and ash clouds, which could endanger overflying aircraft. The volcanoes of southern Peru pose the most significant

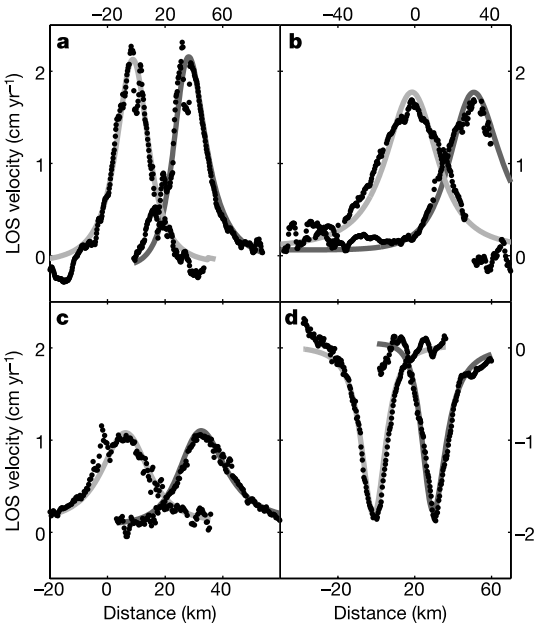

Figure 2 South to north (light grey) and west to east (dark grey) profiles through the interferometric observations (points, same data as shown in Fig. 1 in map insets and model fits (lines), both shown as rates. The west–east profile has been offset for the sake of clarity. The profiles intersect at the centre of their respective deformation patterns. **a**, Hualca Hualca. In these profiles, the data points are consistently below the models owing to a localized region of subsidence to the northeast of Hualca Hualca that is visible in Fig. 1. **b**, Uturuncu. **c**, Lazufre. **d**, Robledo.

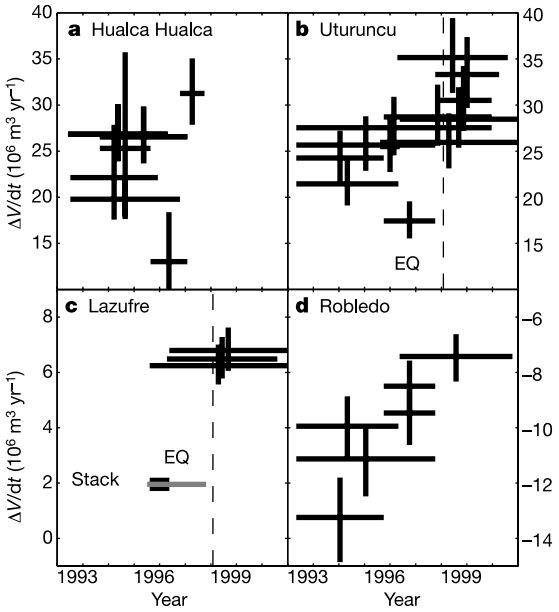

Figure 3 Inferred rate of volume change as a function of time, assuming a constant source depth at each location, a spherically symmetric source in a half-space, and a constant rate of deformation during the time period covered in each interferogram. The horizontal bar shows the time period covered by the interferogram and the vertical bar reflects an estimate of the error on the inferred rate of volume change. The error bar is 0.05 units in log space (such that the absolute error scales with the size of the source), except for scenes with extensive atmospheric contamination at Hualca Hualca, where we estimate the error to be 0.10 log units. The vertical error bar has been estimated by looking at the spread in the scatter plot of misfit as a function of source strength, comparing the strength results from inversions of different combinations of data sets, and comparing interferograms that span nearly the same time interval, including a set of interferograms at Robledo that differ by only one day. **a**, Hualca Hualca. **b**, Uturuncu shows an increase in inflation following a $M_w = 7$ Chilean subduction zone earthquake. The time of the earthquake is shown by a dashed vertical line (labelled EQ). **c**, Lazufre. Two interferograms before 1998 have been averaged (the black and grey horizontal bars labelled Stack represent the time span of the two interferograms) and show no deformation. The stacked data place an upper bound on the rate of source volume change. Three interferograms that include times following the $M_w = 7$ Chilean subduction zone earthquake show deformation. **d**, Robledo. The total volume of material inferred to have moved during the observation period for each source is: Uturuncu, 2.4×10^8 m^3; Robledo, -9×10^7 m^3; Hualca Hualca, 1.3×10^8 m^3; and Lazufre, 3.5×10^7 m^3.

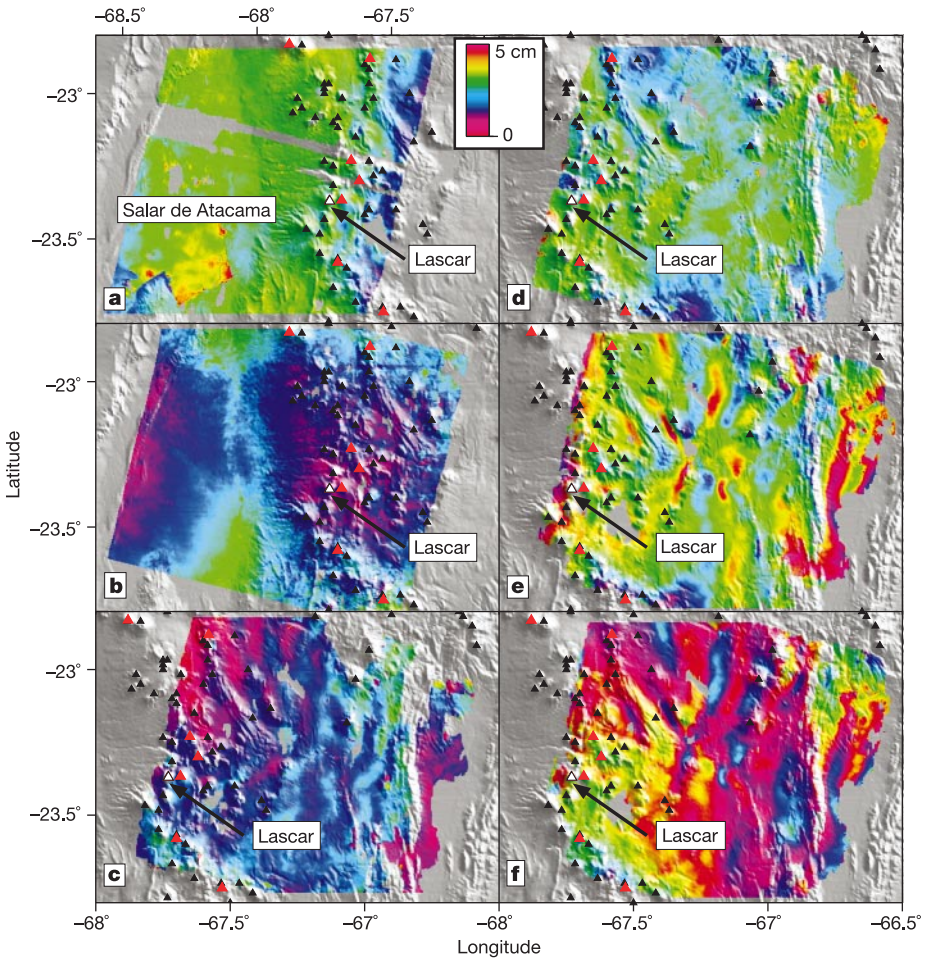

Figure 4 Interferograms showing no deformation at Lascar from two satellite tracks of radar data. Black triangles show volcanic edifices, red triangles are potentially active volcanoes, and the white triangle is Lascar. **a**, 12 August 1995–24 December 2000 (track 282), spanning the 20–21 July 2000, eruption and a quiet vapour emission[6]. Deformation in the Salar de Atacama is clearly visible. **b**, 6 August–19 March 2000 (track 282), spanning the eruption on 20–21 July 2000 (refs 5, 6). **c**, 26 March 1996–13 November 1993 (track 10), spanning the eruption on 17 December 1993 (refs 4, 6, 25), and small eruptions March 1994–June 1995 (ref. 6). **d**, 7 October 1997–2 October 1995 (track 10), during which the only documented activity was a quiet vapour emission[6]. **e**, 2 October 1995–2 May 1992 (track 10) spanning the major eruption on 18–20 April 1993, the eruption on 17 December 1993 (refs 3, 4, 6, 25), and other small eruptions March 1994–June 1995 (ref. 6). **f**, 2 October 1995–2 May 1992 (track 10), spanning the major eruption on 18–20 April 1993 the eruption on 17 December 1993 (refs 3, 4, 6, 25), small eruptions March 1994–June 1995 (ref. 6), and a quiet vapour emission[6].

hazard because of the higher population density in that area. For example, an eruption from Hualca Hualca, Sabancaya or Ampato could endanger the 35,000 people who live near this group of volcanoes[24]. □

Received 30 April; accepted 27 May 2002; doi:10.1038/nature00872.

1. Dvorak, J. J. & Dzurisin, D. Volcano geodesy: The search for magma reservoirs and the formation of eruptive vents. *Rev. Geophys.* **35,** 343–384 (1997).
2. de Silva, S. L. & Francis, P. W. *Volcanoes of the Central Andes* (Springer, New York, 1991).
3. Gonzalez-Ferran, O. *Volcanes de Chile* (in Spanish) (Instituto Geografico Militar, Santiago, Chile, 1995).
4. Matthews, S. J., Gardeweg, M. C. & Sparks, R. S. J. The 1984 to 1996 cyclic activity of Lascar Volcano, northern Chile: Cycles of dome growth, dome subsidence, and explosive eruptions. *Bull. Volcanol.* **59,** 77–82 (1997).
5. Wooster, M. J. Long-term infrared surveillance of Lascar Volcano: Contrasting activity cycles and cooling pyroclastics. *Geophys. Res. Lett.* **28,** 847–850 (2001).
6. Smithsonian Institution Global Volcanism Program. ⟨http://nmnhwww.si.edu/gvp/⟩ (accessed 29 April 2002).
7. Hanssen, R. A. *Radar Interferometry: Data Interpretation and Error Analysis* (Kluwer Academic, Dordrecht, The Netherlands, 2001).
8. Amelung, F., Jonsson, S., Zebker, H. & Segall, P. Widespread uplist and 'trapdoor' faulting on Galapagos volcanoes observed with radar interferometry. *Nature* **407,** 993–996 (2000).
9. Sambridge, M. Exploring multi-dimensional landscapes without a map. *Inverse Problems* **14,** 427–440 (1998).
10. Yuan, X. *et al.* Subduction and collision processes in the Central Andes constrained by converted seismic phases. *Nature* **408,** 958–961 (2000).
11. Wigger, P. J. *et al.* in *Tectonics of the Southern Central Andes: Structure and Evolution of an Active Continental Margin* (eds Reutter, K.-J., Scheuber, E. & Wigger, P. J.) 23–48 (Springer, Berlin, 1994).
12. Williams, C. A. & Wadge, G. The effects of topography on magma chamber deformation models: Application to Mt. Etna and radar interferometry. *Geophys. Res. Lett.* **25,** 1549–1552 (1998).
13. Johnston, M. J. S., Hill, D. P., Linde, A. T., Langbein, J. & Bilham, R. Transient deformation during triggered seismicity from the 28 June Mw = 7.3 Landers earthquake at Long-Valley caldera, California. *Bull. Seismol. Soc. Am.* **85,** 787–795 (1995).
14. de Silva, S. L. Altiplano-Puna volcanic complex of the central Andes. *Geology* **17,** 1102–1106 (1989).
15. Chmielowski, J., Zandt, G. & Haberland, C. The central Andean Altiplano-Puna magma body. *Geophys. Res. Lett.* **26,** 783–786 (1999).
16. Lazo, M., Kosaka, A., Minaya, A., Gonzales, E. & Soto, J. in *Proc. VII Congreso Peruano de Geologia* 19–22 (Sociedad Geologica del Peru, Lima, 1991).
17. Curtis, G. H. in *Studies in Volcanology, a Memoir in Honor of Howell Williams* Geol. Soc. Mem. 116 (eds Coats, R. R., Hay, R. L. & Anderson, C. A.) 153–210 (GSA, Boulder, CO, 1968).
18. Simkin, T. & Siebert, L. *Volcanoes of the World* (Geoscience, Tucson, 1994).
19. Matthews, S. J., Sparks, R. S. J. & Gardeweg, M. C. Piedras Grandes-Soncor eruptions, Lascar volcano, Chile; evolution of zoned magma chamber in the central Andean upper crust. *J. Petrol.* **40,** 1891–1919 (1999).
20. Matthews, S. J., Jones, A. P. & Gardeweg, M. C. Lascar volcano, northern Chile—Evidence for steady-state disequilibrium. *J. Petrol.* **35,** 401–432 (1994).
21. Rymer, H., Murray, J. B., Brown, G. C., Ferrucci, F. & McGuire, W. J. Mechanisms of magma eruption and emplacement at Mt. Etna between 1989 and 1992. *Nature* **361,** 439–441 (1993).
22. Fernandez, J., Tiampo, K. F., Jentzsch, G., Charco, M. & Rundle, J. B. Inflation or deflation? New results for Mayon volcano applying elastic-gravitational modeling. *Geophys. Res. Lett.* **28,** 2349–2352 (2001).
23. Watanabe, H., Okubo, S., Sakashita, S. & Maekawa, T. Drain-back process of basaltic magma in the

summit conduit detected by microgravity observation at Izu-Oshima volcano, Japan. *Geophys. Res. Lett.* **25,** 2865–2868 (1998).
24. Thouret, J.-C. *et al.* Geomorphological and geological survey, and SPOT remote sensing of the current activity of Nevado Sabancaya stratovolcano (south Peru): assessment for hazard-zone mapping. *Z. Geomorph.* **39,** 515–535 (1995).
25. Wooster, M. J. & Rothery, D. A. Thermal monitoring of Lascar Volcano, Chile, using infrared data from the along-track scanning radiometer: a 1992–1995 time series. *Bull. Volcanol.* **58,** 566–579 (1997).

Acknowledgements

European Space Agency (ESA) remote-sensing satellite (ERS) synthetic aperture radar (SAR) imagery for this study was acquired as a Category 1 research project from the ESA. We thank A. Linde for a critical review, L. Rivera and R. Lohman for modelling software, S. de Silva for an electronic version of his volcano database, and H. Zebker, Y. Fialko, P. Segall, E. Brodsky and M. Battaglia for useful discussions. This material is based upon work partially supported by the National Science Foundation under a grant to M.S. M.E.P. was partly supported by NASA and NSF fellowships.

Competing interests statement

The authors declare that they have no competing financial interests.

Correspondence and requests for materials should be addressed to M.E.P. (e-mail: matt@gps.caltech.edu).

Local dispersal promotes biodiversity in a real-life game of rock–paper–scissors

Benjamin Kerr*, Margaret A. Riley†, Marcus W. Feldman* & Brendan J. M. Bohannan*

* *Department of Biological Sciences, Stanford University, Stanford, California 94305, USA*
† *Department of Ecology and Evolutionary Biology, Yale University, New Haven, Connecticut 06511, USA*

One of the central aims of ecology is to identify mechanisms that maintain biodiversity[1,2]. Numerous theoretical models have shown that competing species can coexist if ecological processes such as dispersal, movement, and interaction occur over small spatial scales[1–10]. In particular, this may be the case for non-transitive communities, that is, those without strict competitive hierarchies[3,6,8,11]. The classic non-transitive system involves a community of three competing species satisfying a relationship similar to the children's game rock–paper–scissors, where rock crushes scissors, scissors cuts paper, and paper covers rock. Such relationships have been demonstrated in several natural systems[12–14]. Some models predict that local interaction and dispersal are sufficient to ensure coexistence of all three species in such a community, whereas diversity is lost when ecological processes occur over larger scales[6,8]. Here, we test these predictions empirically using a non-transitive model community containing three populations of *Escherichia coli*. We find that diversity is rapidly lost in our experimental community when dispersal and interaction occur over relatively large spatial scales, whereas all populations coexist when ecological processes are localized.

Microbial laboratory communities have proved useful for studying the generation and maintenance of biodiversity[15–17]. In particular, communities containing toxin-producing (or colicinogenic) *E. coli* have been the centre of much attention from both theoretical ecologists[3,6,8,18–20] and microbiologists[21–27]. Colicinogenic bacteria possess a 'col' plasmid, containing genes that encode the colicin (the toxin), a colicin-specific immunity protein (which renders the cell immune to the colicin) and a lysis protein (which is expressed when the cell is under stress, causing partial cell lysis and the subsequent release of the colicin)[26,27]. In general, only a small fraction of a population of colicinogenic cells will lyse and release the colicin[27]. Colicin-sensitive bacteria are killed by the colicin but may occasionally experience mutations that render them resistant to the colicin. The most common mutations alter cell membrane proteins that bind or translocate the colicin[23,24,26,27]. In some cases, the growth rate of resistant cells (R) will exceed that of colicinogenic cells (C), but will be less than the growth rate of sensitive cells (S). This occurs because resistant cells avoid the competitive cost of carrying the col plasmid[21,22,26,27] but suffer because colicin receptor and translocation proteins are also involved in crucial cell functions such as nutrient uptake[21,23,24,26,27]. In such cases, S can displace R (because S has a growth-rate advantage), R can displace C (because R has a growth-rate advantage) and C can displace S (because C kills S). That is, the C–S–R community satisfies a rock–paper–scissors relationship.

Using a modification of the lattice-based simulation of Durrett and Levin[6], we theoretically explored the role of the spatial scale of

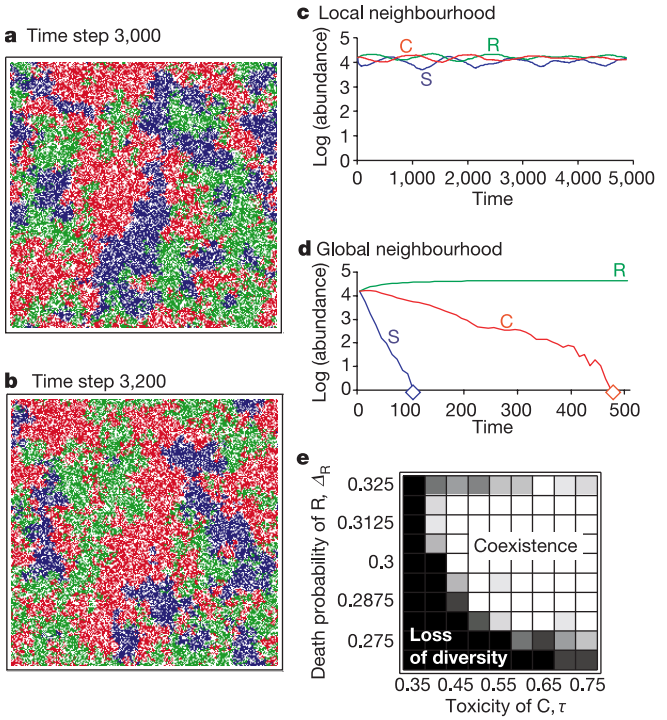

Figure 1 Predictions of the lattice-based simulation (see Box 1). **a**, **b**, Snapshots of the lattice in a simulation with a local neighbourhood at times 3,000 (**a**) and 3,200 (**b**). The unit of time is an 'epoch', equal to 62,500 lattice point updates (an epoch is the average turnover of any given lattice point in the 250 × 250 grid). The strains are colour-coded as follows: C is red, S is blue and R is green; empty lattice points are white. **c**, The complete community dynamics for the same simulation run. **d**, Community dynamics for a simulation with a global neighbourhood. The abundances in **c** and **d** are log transformed. When the abundance of a strain goes to zero, we represent this event with a diamond on the abscissa of the relevant graph at the relevant time. For **a**–**d** we used the following parameters: $\Delta_C = 1/3$, $\Delta_{S,0} = 1/4$, $\Delta_R = 10/32$, and $\tau = 3/4$ (see Box 1). **e**, Sensitivity of qualitative dynamics to changes in a subset of parameter values. For the (τ, Δ_R) values plotted, the greyscale indicates the number of 'local' simulated runs (out of 10) in which coexistence occurred for at least 10,000 epochs, with the lighter area indicating a higher probability of coexistence. For all simulations, we require $\Delta_{S,0} < \Delta_R < \Delta_C < \frac{\Delta_{S,0}+\tau}{1+\tau}$, which (at least for the mixed system) ensures that S displaces R, R displaces C, and (if C has sufficient density) C displaces S.